coatings

MDPI

Article

High Temperature Wear Behavior of Titanium Nitride Coating Deposited Using High Power Impulse Magnetron Sputtering

Chin-Chiuan Kuo [1,*], Yu-Tse Lin [1], Adeline Chan [1] and Jing-Tang Chang [2]

[1] Department of Mechanical and Computer Aided Engineering, National Formosa University, Huwei, Yunlin County 63201, Taiwan
[2] Supati Corporation, Citong, Yunlin County 64747, Taiwan
* Correspondence: cckuo@nfu.edu.tw; Tel.: +886-5631-3492

Received: 16 July 2019; Accepted: 27 August 2019; Published: 29 August 2019

Abstract: Titanium nitride (TiN) coating has been used in various application as it gives excellent performance in many aspects. It has been proven to prolong machining tool life since the mid-1960s. Industrial deposition processes of TiN, including magnetron sputtering, arc ion plating, and chemical vapor depositions, have their individual advantages and limitations. Due to the rising demands of the dry machining technique, the massive amount of heat generated from the friction of cutting tools against the surface of a work piece has become the main issue to overcome. Oxidation of TiN, which occurs around 400 °C, puts a limit on the applications of the coatings. Comparing TiN tool coatings deposited by arc evaporation, the novel high-power impulse magnetron sputtering (HiPIMS) technology provides smoother film surface, denser structure and subsequent corrosion resistance. Therefore, this research aims to investigate the wear behavior of TiN thin film deposited by HiPIMS at high temperature. The influences of the coating properties on the wear resistance of coatings at high temperature are also investigated. The results show that the HiPIMS technique enables a denser epitaxial-grown TiN coating with higher surface hardness and adhesion in contrast with TiN coating deposited using direct current (DC) magnetron sputtering techniques, which provides a higher wear resistance.

Keywords: titanium nitride; high power impulse magnetron sputtering; high temperature wear

1. Introduction

Titanium nitride (TiN) coating and various deposition techniques have been developed in recent decades. TiN has been widely employed in machining and automobile industries because of its remarkable properties, such as high hardness and chemical stability, and low wear rate, friction coefficient and electrical resistivity, which are applied in a wide range of working environments [1–5].

The current commonly used TiN deposition techniques include arc evaporation, magnetron sputtering and chemical vapor depositions. These rival deposition techniques each have individual coating properties and process flexibility. TiN films deposited by chemical vapor deposition usually require a relatively higher process temperature than traditional hardening treatments of most tool steel [1,2]. The process temperature of physical vapor deposition is relatively low compared to chemical vapor deposition. However, TiN coating deposited by the typical magnetron sputtering technique still requires a post-annealing or deposition process temperature of around 400 °C to achieve sufficient hardness [1,3]. Therefore, the high processing temperature becomes a restriction in the choice of substrate materials. Although arc evaporation of TiN is the simplest system with the lowest production cost, numerous embedded microdroplets in the film weakens corrosion resistance and

yields a rougher surface compared with the sputtering deposited coating [6], which may reduce the precision of machining tools and formed molds.

The high power impulse magnetron sputtering (HiPIMS) technique is based on the concept of magnetron sputtering with high power density pulses. The high-power pulses provide a high ionization ratio of the sputtered source material, which enables the feasibility of altering the energy of incident film-forming particles, as well as substrate biasing. This reduces the limitations of substrate temperature and process pressure on the film microstructure and associated film properties [7–9]. Compared with traditional magnetron sputtering, the films deposited by HiPIMS exhibit the same smooth surface but have higher mechanical performance and chemical corrosion resistance [10]. These advantages mean that HiPIMS can be an excellent choice of high-quality coating treatment for high-precision machining tools or molds at a relatively low deposition temperature.

It is known that binary TiN coatings are easily oxidized at a service temperature above 450 °C [11,12]. The current studies of elevated temperature wear behaviors of nitride coatings focus on ternary and quaternary nitrides with better oxidation resistance [11–15]. Since the denser microstructure of HiPIMS-deposited binary TiN coatings can provide better corrosion resistance in an aqueous environment [10], it may also retard oxidation. Therefore, in this research, TiN layers were deposited using HiPIMS and direct current magnetron sputtering (DCMS) onto high speed steel (HSS) substrate. A comparison of the mechanical properties and high temperature wear resistance of both methods (DCMS and HSS) is made.

2. Materials and Methods

TiN films deposited via HiPIMS and DCMS techniques were carried out in the same deposition system with a Hüttinger TruPlasma Unipolar 4001 (TRUMPF, Ditzingen, Germany) plasma power supply. For HiPIMS, the deposition of coating was set to unipolar pulse mode, whereas for DCMS coating, the DC mode of the power source was used for deposition. Substrate bias voltage was applied to the substrate using a TRUMPF Hüttinger TruPlasma Bias 3018 bias power supply. HiPIMS and DCMS deposition parameters of TiN coatings are shown in Table 1.

Table 1. HiPIMS and DCMS deposition parameters of TiN coatings.

Layer	Deposition Mode	HiPIMS	DCMS
Ti Interlayer	Deposition pressure (Pa)	0.56	0.40
	Average target voltage (V)	567	461.1
	Average target current (A)	150.8	7.7
	Average power (kW)	3.5	3.6
	Peak current (A)	171.7	N/A
	Pulse frequency (Hz)	756	N/A
	Pulse time (μs)	55	N/A
	Pulse duty cycle (%)	4.1	N/A
	DC Bias voltage (V)	−800	−800
	Duration (min)	10	2
TiN top-layer	Ar/N_2 gas flow ratio	6:1	4:1
	Average target voltage (V)	578.6	463.12
	Average target current (A)	135.41	7.7
	Average power (kW)	3.5	3.6
	Peak current (A)	193.8	N/A
	Pulse frequency (Hz)	795	N/A
	Pulse time (μs)	55	N/A
	Pulse duty cycle (%)	4.4	N/A
	DC Bias voltage (V)	−70	−70
	Duration (min)	85	25

AISI M35 high speed steel rods with two different diameters, 55 and 30 mm, were cut into 10 mm thick discs. Parts of AISI M35 samples were machined into a size of 11 mm (w) × 18 mm (l) × 4 mm (h). High speed steel (HSS) samples were all quench hardened to HRC 65.8. The hardened AISI M35 substrate was ground, degreased, ultrasonically water rinsed, alcohol rinsed, and air-dried before the deposition. Polished AISI 304 stainless-steel substrates with a size of 20 mm (w) × 30 mm (l) × 1 mm (h) and silicon wafers with a size of 1021 mm^2 (a) × 0.3 mm (h) were also deposited at the same time in the trial deposition. All the substrates of different materials and dimensions were prepared for related further tests or measurements.

The substrates were placed facing the titanium target at a distance of 100 mm in a vacuum chamber. The deposition temperature was kept at a constant 430 °C throughout the deposition. When the base pressure of the vacuum chamber reached 7.97×10^{-3} Pa, argon gas was introduced. The surface of the substrate was argon plasma cleaned by applying a substrate bias of −1000 V at the chamber pressure of 3.55 Pa for 30 min prior to the deposition of the TiN layer. After plasma cleaning, the pressure of the vacuum chamber was further reduced to a working pressure of 0.56 Pa while keeping the substrate bias at −800 V. High voltage pulses were applied to the target to initiate the sputtering of titanium. With Ti^+ ion bombardment for 10 min, a thin layer of Ti interlayer was deposited on the substrates, then different fractions of nitrogen gas were introduced into the chamber for deposition of the TiN layer. The gas ratio of argon to nitrogen for HiPIMS-TiN deposition was 6:1, whereas a ratio of 4:1 was used for DCMS-TiN deposition. A substrate bias of −70 V was maintained during the TiN deposition for both processes. After the trial deposition, the calculated deposition rate of HiPIMS-TiN was 25.3 nm/min and that of DCMS-TiN was 92.6 nm/min. Since the deposition rates of the two processes are quite different, the deposition times were set to obtain a similar thickness of around 2.4 µm. The Ar/N_2 gas flow ratio of the DCMS process was also lowered to increase the nitrogen gas fraction to fulfill the reactions with the higher yield of DC-sputtered Ti species.

Several analyses were conducted to examine and compare the properties of TiN coating deposited by different techniques. An BX60M optical microscope (Olympus, Tokyo, Japan) was used to measure the hardness indents, to evaluate the film adhesion, and to observe the wear tracks. Crystallinity of films was characterized by utilizing a MiniFlex X-ray diffractometer (Rigaku, Tokyo, Japan). An MRI, Raman spectrometer (PROTRUSTECH, Tainan, Taiwan) was used to determine the presence of oxidation in the TiN coating after annealing at different high temperatures. A laser beam with a wavelength of 532 nm was irradiated for an integration time 10 s on the measured area to acquire the Raman peak of oxidized substances that appeared along the wear track of the film annealed at various high temperatures.

Different criteria of mechanical properties of thin film were examined. Thicknesses of thin film were measured by using a Calotest Compact Calotester (CAT^2c, Anton Paar, Graz, Austria). Thickness calculations of the sample were based on the standard EN 1071-2 [16]. The relationship between the thickness of the film, s, and penetration depth is shown in Equation (1):

$$s = \frac{D^2 - d^2}{8R} \tag{1}$$

where D is the ground diameter of the film, d is the ground diameter of the substrate and R is the radius of the ball used in the calotest. The radii of balls were maintained at 75 mm. Thicknesses obtained at 3 locations of the samples were averaged to calculate the average thickness of the film deposited. The surface roughness of coated samples was determined using a Surfcorder SE3500 profilometer (Kosaka Laboratory Ltd., Tokyo, Japan).

High speed steel with a hard coating is a common combination used in machining tools, which usually sustain a higher load on both coating and substrate. In order to easily compare with other industrial coated tools, a microhardness test, which may contain part of the substrate effect and corresponds to the conducted wear test, was undertaken in this work. Microhardness indentations were carried out using a HMV-G Series Micro Hardness Testing Machine (Shimadzu, Tokyo, Japan)

with a load of 0.1 g for 12 s on coated samples. The microhardness value was calculated from the mean of 5 measurements of different locations on one single sample.

To determine the adhesion strength between thin film and substrate, a scratch test and VDI 3198 indentation test were conducted using a Revetest Xpress Scratch Tester (CMS Instrument, Peseux, Switzerland) and HR-400 Rockwell hardness indentation machine (Mitutoyo, Tokyo, Japan), respectively. In the scratch test, 3 scratches were drawn with a linearly increasing load from 0 to 100 N at 10 mm distance to obtain the critical load of fracture and delamination of coatings by accompanying acoustic emission and visual observation. Furthermore, the cracking type of coatings around the edges of Rockwell hardness indents were classified in accordance to the VDI 3198 test [17,18] to determine the adhesion of coatings.

The ball-on-disc abrasive wear tests of coated samples were conducted using an Anton Paar High Temperature Tribometer in accordance with the standard ASTM G 99-17 [19] at various temperatures. DIN 100Cr6 steel balls were used for the wear test at room temperature and Al_2O_3 alumina balls were used for higher temperatures. Alumina balls were chosen rather than steel balls for the high temperature wear test due to the deformation resistance of alumina balls towards heat. During the wear test, a nominal load of 2 N was applied to the ball toward the coated HSS specimens. The test distance at room temperature was 80 and 1000 m at a high temperature.

3. Results and Discussion

The X-ray diffraction patterns of DCMS-TiN coated and HiPIMS-TiN coated specimens are shown in Figure 1. The minor peaks labeled Ferrite/Martensite belong to the HSS substrate. It is not possible to differentiate the ferrite and martensite phases from these weak peaks. The peak intensity of (111) is significant in the TiN coating deposited using DCMS, which indicates the preferred orientation (111). This could be attributed to the lower mobility of titanium adatom and shorter diffusion distance on TiN (111) surface [9,20]. On the contrary, there is no obvious preferred orientation for the TiN coating deposited using HiPIMS. This manifests as a result of higher kinetic energy of adatoms, which leads to an epitaxial growth of fine grain structure [10,21]. It can also be inferred that the high ion-to-atom ratio and high ion bombardment causes recrystallization and epitaxial growth of TiN grains [22]. The presence of a Ti_2N phase in DCMS-TiN indicates insufficient nitrogen gas fraction even though the Ar/N_2 gas flow ratio is higher than that of the HiPIMS process. However, further increase of nitrogen fraction induces intensified arcing due to target poisoning phenomena, which is one of the drawbacks of DC sputtering [7].

Figure 2 shows the cross-sectional scanning electron microscope (SEM, S-4800 Cold Field Emission Scanning Electron Microscope, Hitachi, Tokyo, Japan) SE images of HiPIMS-TiN and DCMS-TiN deposited on silicon wafer. Although the film thicknesses of trial deposited samples vary, the differences of microstructure in both coatings deposited with different systems are obvious. On one hand, the HiPIMS-deposited film exhibited a coarse columnar grain structure, which is in the range of Zone 3 according to the structure zone model proposed by Anders based on Thornton's Structure Zone Model [23]. On the other hand, films deposited using the DCMS system shows featherlike columnar features, which are in the range of Zone 1 to Zone T. The more granular-like structure of HiPIMS-TiN supports the previously mentioned observation regarding higher kinetic energy of adatoms than of DCMS, as the deposition process proceeded at the same substrate temperature.

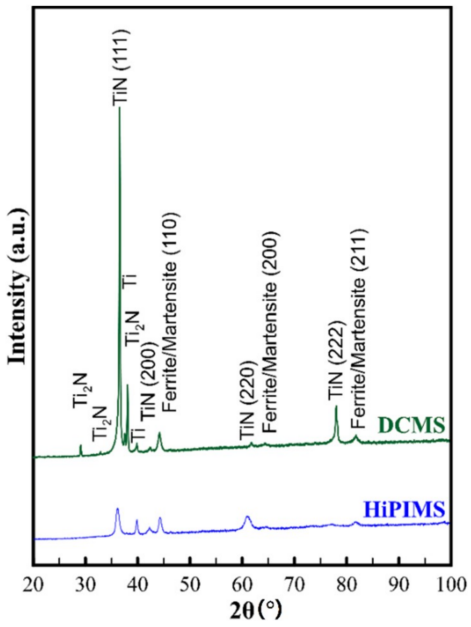

Figure 1. X-ray Diffraction (XRD) spectra of TiN deposited on high speed steel (HSS) using HiPIMS and DCMS techniques.

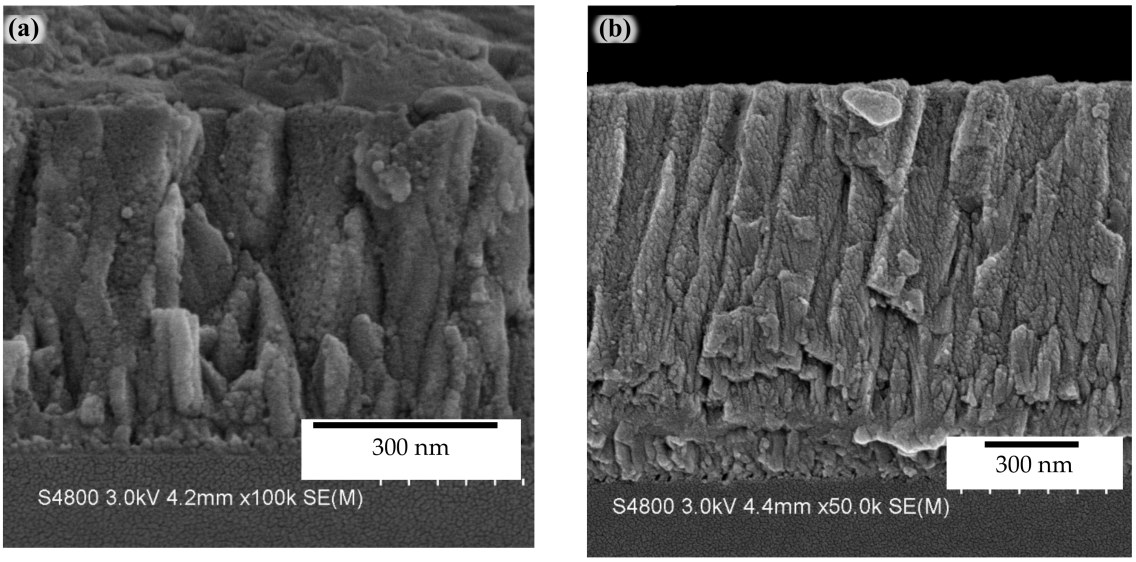

Figure 2. Cross-sectional SE micrographs of TiN deposited by (**a**) HIPIMS and (**b**) DCMS on silicon wafer.

Based on these results, it can be inferred that HiPIMS coatings with a denser, epitaxial granular structure are stiffer than DCMS coatings. This inference can be found in many studies [7,10]. The conjecture correlates to the hardness discussed in the following comparison of the mechanisms of TiN deposited by HiPIMS and DCMS. The denser film structure with less defects, such as column boundaries and pores, may suppress the diffusion of corrosive substances and result in better corrosion and oxidation resistance of HiPIMS-TiN coating [10].

3.1. Comparison of Mechanical Properties and Wear Behaviors of TiN Coatings at Room Temperature

The measured Vicker's hardness value of TiN coating deposited by HiPIMS is 1415 HV, whereas that of TiN coating deposited by DCMS is 942 HV. Although the hardness values are greatly influenced by the relatively softer substrate, there are significant differences between specimens of the two

processes. Such a great difference could be attributed to the composition and the density of the film. The XRD pattern of DCMS shows that the presence of a minor Ti_2N phase could be the reason for the decrease of the hardness of the films.

The adhesion strength of both TiN coatings was determined by undertaking a scratch test based on the standard test method ASTM G99-17 [19]. The HiPIMS-TiN and DCMS-TiN specimens exhibit adhesion strengths of 53 and 17 N, respectively. In addition to the scratch test, the adhesion strength between coating and substrate can also be evaluated by applying Rockwell indentation according to the VDI 3198 norm [18]. Figure 3 shows the optical micrographs of Rockwell indents, with radial microcracks around the indent on HiPIMS-TiN (Figure 3a) with minor delamination. The radial microcrack indicates the film is brittle, and the minor delamination indicates the adhesion is higher than the fracture strength of the brittle TiN coating. Similar results were shown in previous research by Chang et.al [24]. The radial microcracks on DCMS-TiN (Figure 3b) are extremely short and narrow. The DCMS-TiN films are concentrically rippled with deformed HSS substrate, which implies a relatively softer film. Thus, both failure modes of two coatings can be classified to the HF2 level. Although the adhesion strength of DCMS-TiN film measured by the scratch test is much lower than that of HiPIMS-TiN, DCMS-TiN, which is relatively soft yet tough, remained on the substrate without any delamination in the VDI 3198 evaluation. The surface roughness of the HiPIMS and DCMS coatings were 0.1 and 0.09 µm, respectively, which can be mainly attributed to the polishing procedures of HSS. The tested and measured mechanical properties at room temperature are listed in Table 2.

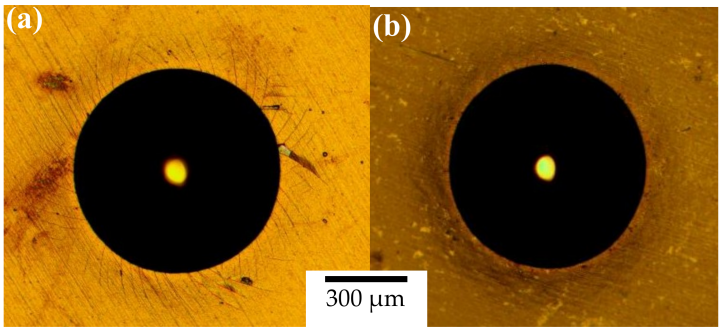

Figure 3. Optical micrograph for Rockwell indents on TiN coatings deposited by (**a**) HiPIMS and (**b**) DCMS onto high speed steel.

Table 2. Comparison of mechanical properties at room temperature between TiN deposited by HiPIMS and DCMS techniques.

Property	HiPIMS	DCMS
Vickers microhardness, $HV_{0.1g.f.}$	1415	942
Adhesion strength (N)	53	17
Failure type (VDI 3198 indentation)	HF 2	HF 2
Roughness, R_a (µm)	0.1	0.09

Room temperature sliding wear tests were carried out using a ball-on-disc tribology method with a DIN 100Cr6 steel ball. From the trendline revealed in the results as shown in Figure 4, the mean friction coefficient of TiN coating deposited using HiPIMS was lower than that of using DCMS. The friction coefficient of DCMS-TiN suddenly dropped at the beginning and then moderately increased to a constant value. The friction coefficient of HiPIMS-TiN was lower in the beginning and then increased in stages, before finally falling to a constant value after a distance of 37 m. Moreover, by comparing the width of wear tracks shown in Figure 5, the track on the DCMS deposited TiN coating is 398.67 µm wide, which is wider than the track on HiPIMS-TiN of 374.9 µm. This reflects the deeper wear track and more severe wear loss of DCMS-TiN coatings. In Figure 5a, scratches of the exposed substrate

were discontinuous as observed in Figure 5b, and the scratches of the exposed substrate were in continuous form. Discontinuously exposed substrate implies higher abrasive penetration resistance of film, which could be attributed to a higher hardness [15,25]. This partially explains the variation of friction coefficient shown in Figure 4. The DCMS-TiN coating might be less resistant to wear, due to its lower hardness, and presents a decrease in friction. However, the HiPIMS-TiN sustains a longer wear distance and causes an increase of friction at early wear stage.

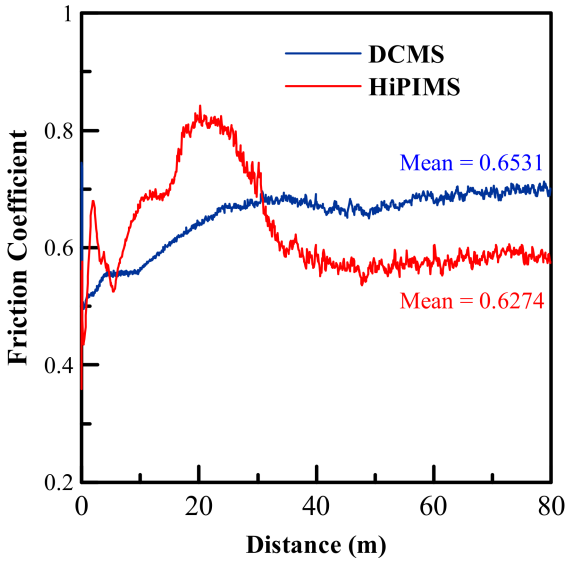

Figure 4. Variations of friction coefficient with sliding distance for two different TiN coated HSS. The ball-on-disc abrasive test was conducted at room temperature condition with a 100Cr6 steel ball.

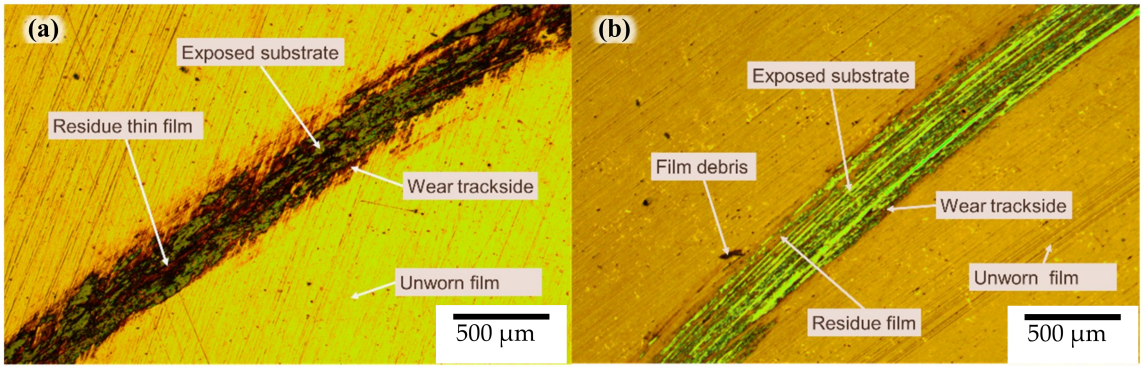

Figure 5. Optical micrograph of wear tracks of TiN coatings deposited by (**a**) HiPIMS and (**b**) DCMS. The ball-on-disc abrasive test was conducted under room temperature condition with a 100Cr6 steel ball.

3.2. Comparison of Wear Behaviors of HiPIMS TiN Coatings at Different Test Temperatures

The high temperature wear test of HiPIMS-TiN was conducted at 150, 300, 450 and 600 °C, respectively. The ball material was replaced by Al_2O_3, which is stable at a high temperature. Variations of friction coefficient with sliding distance at different temperatures are shown in Figure 6. From the trendline, as test temperature increases, the average friction of the alumina ball against the HiPIMS TiN coating decreased gradually. Although the curve at 600 °C presents the lowest average friction coefficient, the coating has the highest friction coefficient between the wear distance of 0 and 8 m. A similar trend can be found in the relationship curves of the average friction coefficient, the surface roughness, and the test temperature shown in Figure 7. This implies that the surface roughness of HSS may be one of the major factors that influences the friction coefficient. However, the surface roughness depends on the polishing of steel substrate rather than the coating. The surface hardness of the unworn

area on coatings heated at different temperatures is listed in Table 3. The annealing process enhanced the surface hardness of TiN coatings due to adjustment of internal stress, grain recrystallization, or defect healing by thermally formed oxides [6].

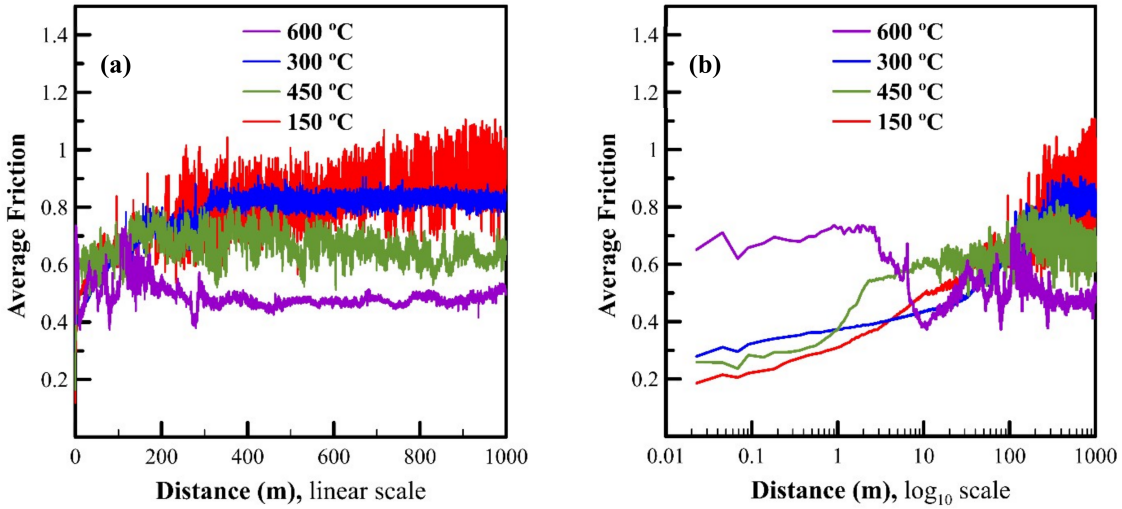

Figure 6. Variations of friction coefficient with sliding distance for HiPIMS-TiN coated HSS tested at different temperatures: (**a**) linear x-axis, (**b**) logarithmic *x*-axis. The ball-on-disc abrasive test was conducted at various temperatures with an Al_2O_3 ball.

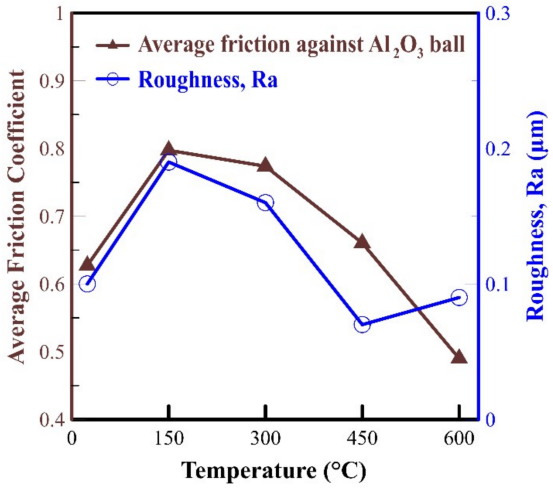

Figure 7. Relationship curves between the average friction coefficient, the surface roughness, and the wear test temperatures.

Table 3. Abrasive processes at high temperatures result in different effects on the mechanism properties of coatings.

Temperature (°C)	Wear Track Width (μm)	Vickers Microhardness (HV)
150	269	1488
300	281	1568
450	391	1392
600	442	N/A

It is known that the oxidation of TiN usually occurs above 400 °C [14,26]. The formation of titanium oxides dominates the wear behavior of TiN coatings at temperatures above 400 °C. The nitride surface of the specimen tested at 450 °C oxidized and transformed to the amorphous nitride-oxide layer,

which smooths the coating surface but weakens the coating hardness. Oxidation and interdiffusion accelerated as the temperature increased further. The higher surface roughness of the specimen tested at 600 °C could be induced by the grain growth of oxide or the pores. The facet of grown oxide may cause protrusions and the interdiffusion of atoms may cause voids and pores [12,13]. Other evidence of the oxidation failure of the specimen tested at 600 °C is provided by the hardness test result. The indent on the specimen tested at 600 °C is unrecognizably severely fractured. The fracture strength of oxidized layer could be serious damaged by the void and pores [12]. The wear behavior of the specimen tested at 600 °C in Figure 6b also supports the hardness result. A rapid drop of the average friction coefficient can be observed at the distance of 1 m. The alumina ball completely penetrates the oxidized TiN coating, and wears against the high-speed steel substrates directly between the distances of 1 and 10 m.

The wear tracks and Rockwell indentation on the HiPIMS-TiN coated specimens tested at different temperatures are shown in Figure 8. Formation of an oxide layer can be observed from the color change from golden to purple-red when the temperature is over 450 °C. The HSS substrate is exposed in the wear track of the specimen tested at 150 °C (Figure 8a). This reflects the significant oscillation of the increasing friction coefficient at the end of test. The indent on the specimen of 150 °C presents a low film adhesion feature. The reason for poor adhesion is not clear. The specimen of 300 °C presents a strong film adhesion. The film is not oxidized or penetrated (Figure 8b). The different colors between the unworn part and the wear track shown in Figure 8c reveal oxidization occurred on the TiN surface. The TiN layer has not been penetrated completely but the track width is broader than that of the 300 °C specimen. This illustrates that oxidation weakens the strong structure of TiN and may accelerate the wear rate of coating. The wear track of the specimen of 600 °C has been penetrated thoroughly, and the coating adhesion becomes poor (Figure 8d). Spallation can be observed on the indent of the TiN coating, showing that the thin film is almost completely oxidized at 600 °C. The porous structure of brittle oxides is easily fractured during the wear test.

The Raman spectra of unworn parts of HiPIMS-TiN coating after testing at different temperatures are shown in Figure 9. The coatings of room temperature, 150 °C, and 300 °C specimens only exhibit scattering peaks of TiN. The spectrum of the specimen of 450 °C exhibits scattering peaks of TiN and anatase TiO_2. As the temperature further increases to 600 °C, the anatase TiO_2 transforms into a relatively thermodynamic stable rutile TiO_2 phase [27]. The scattering of TiN is difficult to identify. However, these results were evidence of the previous discussions.

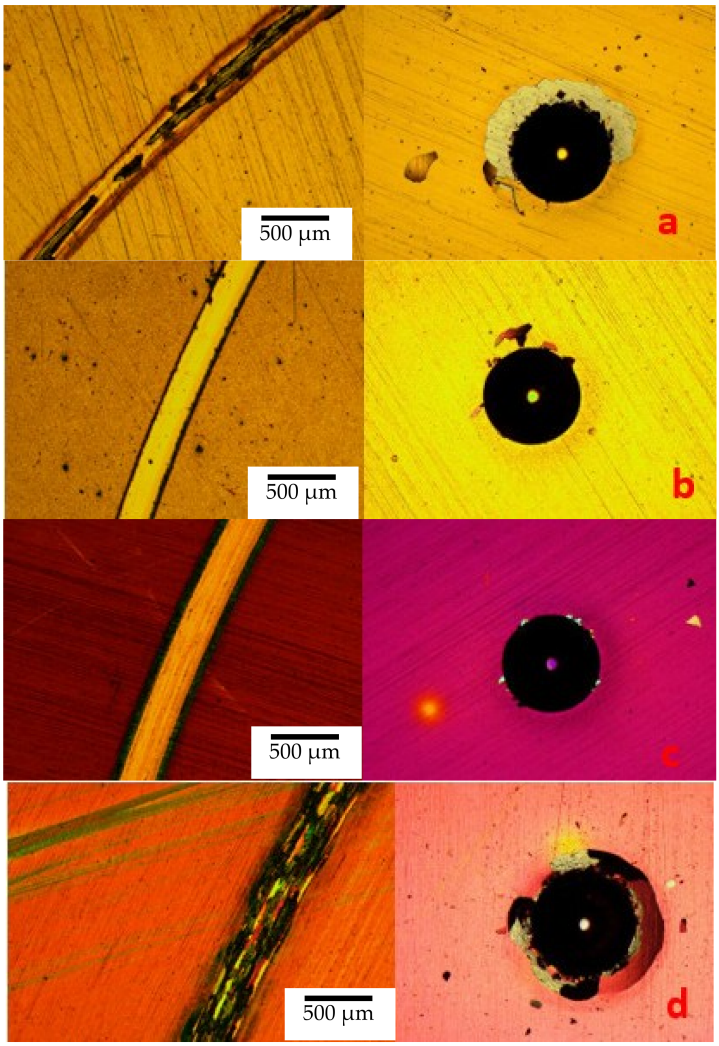

Figure 8. Wear tracks and Rockwell indentations of HiPIMS-TiN coating after testing at the temperatures: (**a**) 150 °C; (**b**) 300 °C; (**c**) 450 °C; and (**d**) 600 °C.

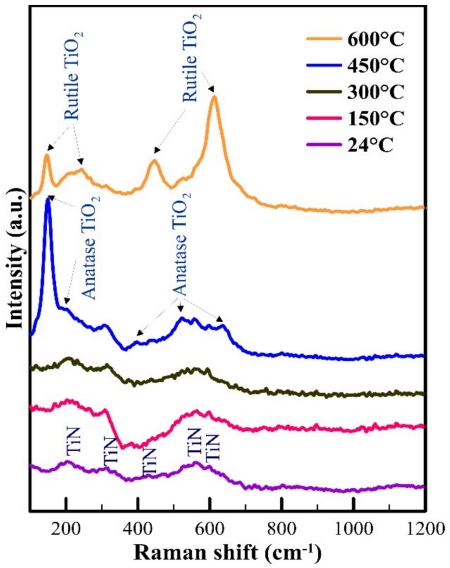

Figure 9. Raman spectra of HiPIMS-TiN coatings annealed at different temperatures.

3.3. Comparison of Mechanical and Wear Behavior Between TiN Coatings Deposited by Different Techniques Annealed at 300 °C

Since the HiPIMS-TiN coating displays the best wear resistance at 300 °C without oxidation, the wear test of DCMS-TiN coating was also undertaken for comparing the two coatings. The mechanical properties of TiN coatings deposited by the two processes after annealing at 300 °C are listed in Table 4. Compared with the results at room temperature in Table 2, the microhardness of DCMS-TiN significantly increased from 942 to 1277 HV after 300 °C annealing. This could be due to recrystallisation, further phase transformation, or formation of oxides.

Table 4. Comparison of the mechanical properties of HiPIMS and DCMS TiN coated samples annealed at 300 °C.

Property	HiPIMS-TiN	DCMS-TiN
Thickness (μm)	2.4	2.5
Microhardness ($HV_{0.1g.f.}$)	1568	1277
VDI 3198 indentation test	HF 3	HF 1
Surface roughness (μm)	0.16	0.07
Width of wear track (μm)	281.09	304.14

The relationship between the friction coefficient and sliding distance of the two types of TiN coatings in the ball-on-disc wear test is shown in Figure 10. The HiPIMS coating has a slightly higher friction coefficient, with a mean value of 0.7738, compared to DCMS coating. However, the DCMS-TiN coating displays a sudden increase at the beginning. Figure 11 shows the micrograph of the wear track of DCMS-TiN tested at 300 °C. The appearance of the wear track is similar to that at room temperature (Figure 5b), where continuous scratches with exposed HSS substrate can be observed. Otherwise, there is no exposed substrate found in the wear track of HiPIMS-TiN, as shown in Figure 8b. These results again provide evidence that TiN coatings deposited using HiPIMS exhibit stronger hardness, higher adhesion strength, and higher temperature tolerance than those using DCMS.

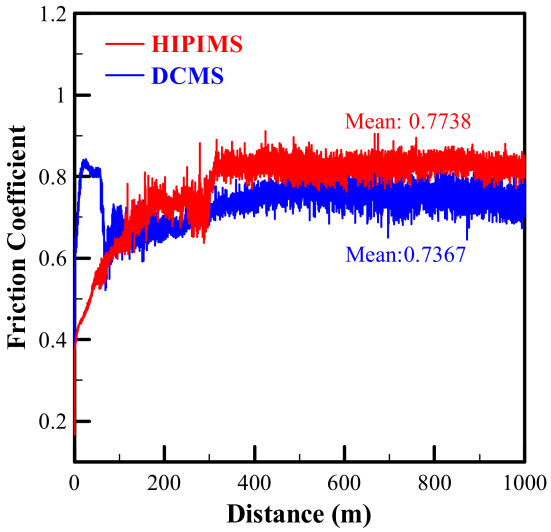

Figure 10. Variation of friction coefficient with sliding distance for HiPIMS-TiN and DCMS-TiN coated HSS wear tested at 300 °C.

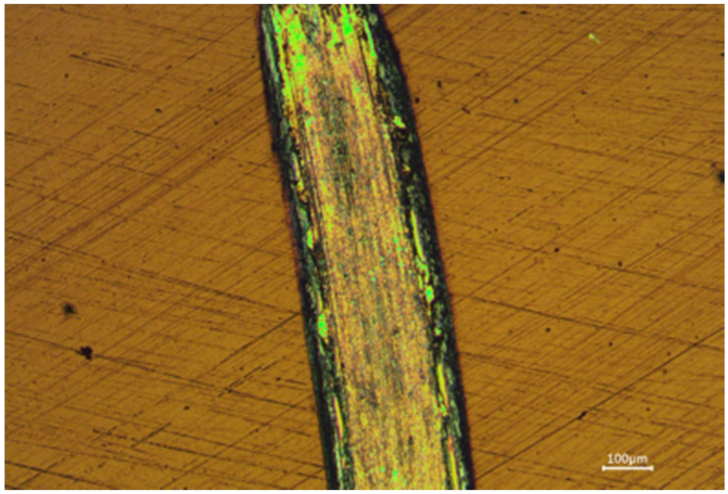

Figure 11. Wear track of DCMS-TiN deposited HSS tested at 300 °C. The wear track of HiPIMS-TiN tested at 300 °C can be referred to in Figure 8b.

4. Conclusions

This research focuses on the effects of thermal oxidation on the mechanical properties and wear behavior of TiN coating deposited using high power impulse magnetron sputtering. The TiN coating deposited by direct current magnetron sputtering is also analyzed. TiN coating deposited by HiPIMS has exceptional wear resistance and mechanical properties compared to DCMS coating.

TiN coating deposited by HiPIMS shows excellent mechanical properties and wear resistance at 300 °C. Although the HiPIMS-TiN surface is unavoidably oxidized above 450 °C, at 450 °C the TiN beneath the oxidized surface layer maintains the mechanical properties of the coating. When the temperature is elevated to 600 °C, the TiN layer completely oxidizes and is easily cracked.

Author Contributions: Conceptualization, C.-C.K.; Methodology, J.-T.C.; Resources, Y.-T.L.; Data Curation, A.C.; Investigation, A.C.; Writing—Original Draft Preparation, A.C.; Writing—Review and Editing, J.-T.C.; Visualization, J.-T.C.; Supervision, C.-C.K.; Project Administration, C.-C.K.; Funding Acquisition, Y.-T.L.; Resource, Y.-T.L.

Funding: This research received no external funding.

Acknowledgments: The authors wish to thank Supati Cooperation for financial support. Plasma Engineering Lab at Department of Materials Science and Engineering, and Precision Instrument Support Center, of Feng Chia University are also acknowledged for the microstructure analysis instruments.

Conflicts of Interest: The authors declare no conflict of interest.

References

1. Zhang, S.-Y.; Zhu, W.-G. TiN coating of tool steels: A review. *J. Mater. Process. Technol.* **1993**, *39*, 165–177. [CrossRef]
2. Faltermeier, C.; Goldberg, C.; Jones, M.; Upham, A.; Manger, D.; Peterson, G.; Lau, J.; Kaloyeros, A.E.; Arkles, B.; Paranjpe, A. Barrier properties of titanium nitride films grown by low temperature chemical vapor deposition from titanium tetraiodide. *J. Electrochem. Soc.* **1997**, *144*, 1002–1008. [CrossRef]
3. Sproul, W.D. Physical vapor deposition tool coatings. *Surf. Coat. Technol.* **1996**, *81*, 1–7. [CrossRef]
4. Sundgren, J.E. Structure and properties of TiN coatings. *Thin Solid Films* **1985**, *128*, 21–44. [CrossRef]
5. Chavda, M.R.; Dave, D.P.; Chauhan, K.V.; Rawal, S.K. Tribological characterization of TiN coatings prepared by sputtering. *Procedia Technol.* **2016**, *23*, 36–41. [CrossRef]
6. Tkadletz, M.; Mitterer, C.; Sartory, B.; Letofsky-Papst, I.; Czettl, C.; Michotte, C. The effect of droplets in arc evaporated TiAl/TaN hard coatings on the wear behavior. *Surf. Coat. Technol.* **2014**, *257*, 95–101. [CrossRef]
7. Anders, A. Tutorial: Reactive high power impulse magnetron sputtering (R-HiPIMS). *J. Appl. Phys.* **2017**, *121*, 171101. [CrossRef]

8. Kouznetsov, V.; Macak, K.; Schneider, J.; Helmersson, U.; Petrov, I. Hybrid HIPIMS and DC magnetron sputtering deposition of TiN coatings: Deposition rate, structure and tribological properties. *Surf. Coat. Technol.* **1999**, *12*, 290. [CrossRef]
9. Machunze, R.; Ehiasarian, A.; Tichelaar, F.; Janssen, G.; Ehiasarian, A. Stress and texture in HIPIMS TiN thin films. *Thin Solid Films* **2009**, *518*, 1561–1565. [CrossRef]
10. Elmkhah, H.; Attarzadeh, F.; Fattah-alhosseini, A.; Kim, K.H. Microstructural and electrochemical comparison between TiN coatings deposited through HIPIMS and DCMS techniques. *J. Alloy. Compd.* **2018**, *735*, 422–429. [CrossRef]
11. Panjan, P.; Navinsek, B.; Cekada, M.; Zalar, A. Oxidation behaviour of TiAlN coatings sputtered at low temperature. *Vacuum* **1999**, *53*, 127–131. [CrossRef]
12. Chen, H.-Y.; Lu, F.-H. Oxidation behavior of titanium nitride films. *J. Vac. Sci. Technol. A* **2005**, *23*, 1006–1009. [CrossRef]
13. Zhang, S.; Sun, D.; Zeng, X.-T. Oxidation of Ni-toughened nc-TiN/a-SiN_x nanocomposite thin films. *J. Mater. Res.* **2005**, *20*, 2754–2762. [CrossRef]
14. Chang, Y.-Y.; Weng, S.-Y.; Chen, C.-H.; Fu, F.-X. High temperature oxidation and cutting performance of AlCrN, TiVN and multilayered AlCrN/TiVN hard coatings. *Surf. Coat. Technol.* **2017**, *332*, 494–503. [CrossRef]
15. Huang, X.; Etsion, I.; Shao, T. Effects of elastic modulus mismatch between coating and substrate on the friction and wear properties of TiN and TiAlN coating systems. *Wear* **2015**, *338*, 54–61. [CrossRef]
16. Comite Europeen de Normalisation. *Advanced Technical Ceramics—Methods of Test for Ceramic Coatings—Part 2: Determination of Coating Thickness by the Crater Grinding Method*; EN 1071-2; Comite Europeen de Normalisation: Brussels, Belgium, 2002.
17. Vidakis, N.; Antoniadis, A.; Bilalis, N. The VDI 3198 indentation test evaluation of a reliable qualitative control for layered compounds. *J. Mater. Process. Technol.* **2003**, *143*, 481–485. [CrossRef]
18. Deutsches Institut fur Normung E.V. (DIN). *Coating (CVD, PVD) of Cold Forging Tools*; DIN VDI 3198; Deutsches Institut fur Normung E.V. (DIN): Berlin, Germany, 1992.
19. ASTM International. *Standard Test Method for Wear Testing with a Pin-On-Disk Apparatus*; ASTM G99-17; ASTM International: West Conshohocken, PA, USA, 2017. [CrossRef]
20. Gall, D.; Kodambaka, S.; Wall, M.A.; Petrov, I.; Greene, J.E. Pathways of atomistic processes on TiN (001) and (111) surfaces during film growth: An ab initio study. *J. Appl. Phys.* **2003**, *93*, 9086–9094. [CrossRef]
21. Alami, J.; Maric, Z.; Busch, H.; Klein, F.; Grabowy, U.; Kopnarski, M. Enhanced ionization sputtering: A concept for superior industrial coatings. *Surf. Coat. Technol.* **2014**, *255*, 43–51. [CrossRef]
22. Mahieu, S.; Depla, D. Reactive sputter deposition of TiN layers: Modelling the growth by characterization of particle fluxes towards the substrate. *J. Phys. D Appl. Phys.* **2009**, *42*, 053002. [CrossRef]
23. Anders, A. A structure zone diagram including plasma-based deposition and ion etching. *Thin Solid Films* **2010**, *518*, 4087–4090. [CrossRef]
24. Chang, C.-L.; Ho, C.-T.; Chen, P.-H.; Chen, W.-C.; Wang, D.-Y.; Wu, W.-Y. Synergetic effect for improved deposition of titanium nitride films. *Surf. Coat. Technol.* **2018**, *350*, 1098–1104. [CrossRef]
25. Łępicka, M.; Grądzka-Dahlke, M.; Pieniak, D.; Pasierbiewicz, K. Tribological performance of titanium nitride coatings: A comparative study on TiN-coated stainless steel and titanium alloy. *Wear* **2019**, *422–423*, 68–80. [CrossRef]
26. Zhao, H.J.; Mi, P.-B.; Ye, F.-X. Compared the oxidation behavior of TiN and TiN/W_2N ceramic coatings during heat treatment. *Mater. Chem. Phys.* **2018**, *217*, 445–450. [CrossRef]
27. Aniołek, K. The influence of thermal oxidation parameters on the growth of oxide layers on titanium. *Vacuum* **2017**, *144*, 94–100. [CrossRef]